Available online at www.sciencedirect.com

jmr&t Journal of Materials Research and Technology

journal homepage: www.elsevier.com/locate/jmrt

Original Article

# Modeling of cutting force and final thickness for low stiffness 2024-T3 aluminum alloy part milling considering its geometry and fixtures

*Mikel Casuso* [a,*], *Antonio Rubio-Mateos* [a], *Fernando Veiga* [a,b], *Aitzol Lamikiz* [c]

[a] *TECNALIA, Basque Research and Technology Alliance (BRTA), Parque Científico y Tecnológico de Guipúzcoa, Donostia-San Sebastián 20009, Spain*

[b] *Departamento de Ingeniería, Universidad Pública de Navarra, Edificio Departmental Los Pinos, Campus Arrosadía, Pamplona 31006, Spain*

[c] *Department of Mechanical Engineering, University of the Basque Country (UPV/EHU), Bilbao Faculty of Engineering, Plaza Torres Quevedo 1, Bilbao 48013, Spain*

ARTICLE INFO

*Article history:*
Received 15 July 2022
Accepted 15 October 2022
Available online 20 October 2022

*Keywords:*
AA 2024 T3 aluminum alloy
Force modeling
Thin floor
Thin parts milling

ABSTRACT

The aeronautic industry is facing many challenges regarding the lifetime, weight and accuracy that aircraft skins must comply to meet stringent structural and aerodynamic requirements. Currently, mechanical milling of aircraft skin parts of 2024-T3 aluminum alloy is displacing the highly pollutant chemical milling. Consequently, flexible and reconfigurable vacuum holding fixtures are being increasingly employed, because they are adaptable to several part geometries, but, since their rigidity is extremely reduced, the low stiffness of parts limits severely their deployment. Aiming to harness the full potential of these holding systems for aluminum alloy skin parts, a complete analysis of final thickness achieved and cutting force is developed. Thin floor parts of different geometries are pocket milled, simply screwed at their corners, emulating a skin part supported by four vacuum cups. Process forces are continuously monitored, and final thickness is measured. It has been proven that the reduction of mass and stiffness during milling causes a corresponding reduction of the natural frequencies of the parts. Also, as long as natural frequencies are not excited, final thickness error is almost constant and not affected by the tool position, but only by the initial geometry and fixtures distribution of the part. Additionally, a new cutting force model for skin parts is empirically calculated. Unlike models designed for fully supported parts, this model is designed for skins held in flexible fixtures. It has a relative error of 5.6% and it allows to optimize the trajectory, geometry and support distribution, thus boosting the use of flexible fixtures.



* Corresponding author.
E-mail address: mikel.casuso@tecnalia.com (M. Casuso).

https://doi.org/10.1016/j.jmrt.2022.10.070

**Nomenclature**

| | |
|---|---|
| $a_p$ | Axial immersion |
| $a_e$ | Radial immersion |
| $d$ | Distance between fixturing points |
| $D_{near}$ | Ratio of the distance from the tool position to the nearest fixturing point regarding the distance from the center of the part |
| $f_z$ | Feed per tooth |
| $\hat{F}$ | Forecasted force values |
| FRF | Frequency response function |
| $h$ | Part initial thickness |
| MAE | Mean absolute error |
| MAPE | Mean absolute percentage error |
| MRR | Material removal rate |
| S | Spindle speed |
| SLD | Stability lobes diagram |
| UHF | Universal holding fixture |
| $V_{rem}$ | Ratio of the remaining volume of the part at the tool position regarding the initial part volume |
| Z | Number of teeth |

## 1. Introduction

Aircraft skin manufacturing is a challenging and demanding issue, due to the high amounts of material, time and energy that entails and the quality and tolerance requisites that are imposed to these skins. A common material for these parts is aluminum alloy 2024-T3, whose use is widespread among aeronautic manufacturers due to its excellent mechanical properties and its suitability meeting aeronautic requirements [1]. Aluminum alloy skins can be fuselage parts, wings, shells, bulkheads and doors, where pockets are machined in order to reduce their weight [2]. Chemical milling was the traditional technology employed for that purpose, but it is highly hazardous and water contaminant, so it is being replaced by mechanical milling [3]. Even so, mechanical milling must still address significant challenges in order to become a feasible and competitive technology in the field of aircraft skins.

The thickness of these aircraft skins is ultra low and consequently so is its stiffness, thus leading to an easy appearance of chatter and forced vibration during mechanical milling, as well as static deflection [4,5] and thermal stresses [6]. They cause aggravated tool wear, reduced spindle life and poor surface quality [7,8]. The last problem is especially critical, as aircraft components must comply with the stringent requirements and tolerances that are imposed due to aerodynamic considerations [9].

**Table 1 – Geometry range of milled parts.**

| | |
|---|---|
| Part thickness ($h$) | 2.03–3.18 – 4.83 mm |
| Part area | 85 × 85–155 × 155–225 × 225 $mm^2$ |
| Distance between fixturing points ($d$) | 69–139 – 209 mm |

Several technologies have been developed to cope low stiffness of skin parts during milling, such are mirror milling and fixture systems. Mirror milling is composed of two 5-axis heads moving synchronously along the skin, one opposite to the other. The first one mills the skin while the second one supports it increasing the stiffness and assuring correct thickness [10]. Nevertheless, mirror milling still entails high investment costs, so it is not feasible for all kinds of skin parts.

On the other hand, there is a great variety of fixture systems [11]. A moving magnetic clamping device that supports the skin has been developed [12]. Another solutions include elastomer layers that clamp the part and dampen the machining process, as a neoprene-based device [13] and a nitrile butadiene vacuum table, able to clamp different kinds of parts and to mitigate vibrations [14].

However, the most usual industrial solution is still vacuum holding fixtures [15], particularly for large skin parts. They can be rigid and specific for a given skin part, or flexible and reconfigurable for different skin geometries [16]. The first ones achieve better final accuracy, but they are less versatile and therefore costlier. Many parts in the aircraft industry are manufactured in low batches, which makes rigid fixtures not applicable for them [17]. On the contrary, flexible holding fixtures can be adapted for different kinds of parts and geometries [18]. They usually consist of a bed of actuators with a vacuum cup at the top holding the skin, as the so-called Universal Holding Fixture (UHF). Some of them consist of a modular solution, such as the one developed by MTorres [19], which also includes a module for thickness measurement; and other devices are a bed or grid of actuators. Companies such as Modig [20], Kostyrka [21] and CMS [22] have developed this kind of devices, designing them also for cutting, drilling and trimming. On the other hand, Onexia provides a universal holding fixture for aircraft parts, but it is focused on composite materials, and for activities such as routing, drilling and water jet cutting [23]. Finally, Burdinberri creates vacuum tools for supporting the skins during manual trimming [24].

One important disadvantage for the complete deployment of universal holding fixtures for milling is their extremely reduced rigidity, as well as the ultra-low stiffness of the skins [25], which forces to increase the number of actuators aiming to reduce unsupported area [26]; or that directly limits their use for trimming, drilling and cutting only [27]. An analysis regarding the influence of milling conditions and tool position

**Table 2 – Followed stages.**

| | First Stage | Second Stage |
|---|---|---|
| Task performed | Preliminary tests | Milling tests |
| Purpose | Optimal milling conditions determination | Force model determination<br>Thickness error analysis |
| Measurement instruments | Accelerometer<br>Impact hammer<br>Dynamometer table | Dynamometer table<br>Thickness gauge |
| Measured signals | Cutting forces<br>Frequency Response Function | Cutting forces<br>Frequency Response Function<br>Final part thickness |

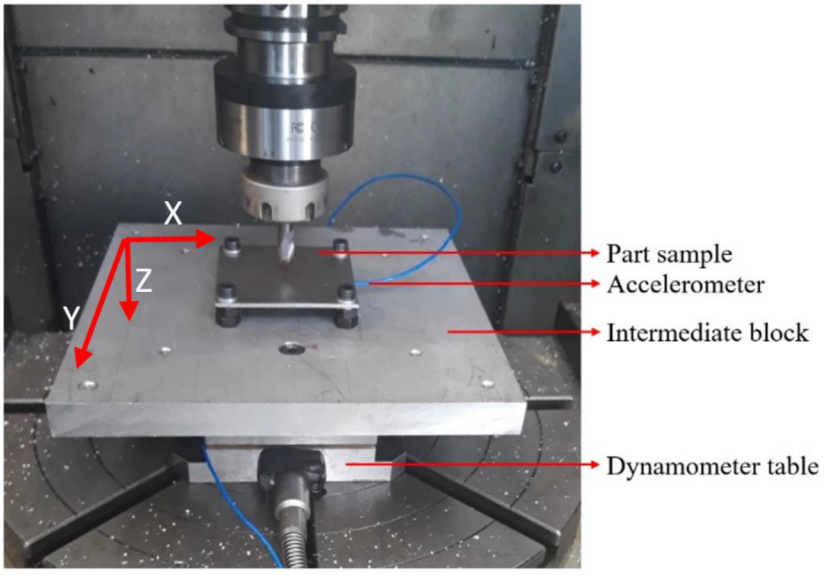


**Fig. 1 – Part of 85 × 85 × 2.03 mm$^3$ simply supported by four screws at its corners and ready for milling with the accelerometer placed below.**

on surface roughness and process vibration in a layout of such a low rigidity has been conducted [28], but there is still a need for a complete force model and a deeper analysis on achieved final thickness in end-milling operation, since cutting force is a key parameter which greatly influences tool wear, part deflection and surface quality [29], and the last two ones are critical values for aeronautic tolerances and requisites.

The present study tries to harness the full potential of flexible and reconfigurable holding systems, developing an empirical model able to forecast the cutting forces that happen in them. For that purpose, thin floors of different geometries have been pocket milled, simply screwed at their corners, emulating a skin part supported by four actuators. In a first stage the optimum milling conditions are determined, and in a second stage these conditions are employed in a full-factorial set of experiments for milling several thin floor parts. Meanwhile, cutting forces are continuously monitored, and thickness error is measured after milling. The purpose is to determine the dimensional factors that mostly affect force and thickness error by means of an analysis of variance, as well as to empirically obtain the mathematical model able to predict cutting force, which will make it possible to optimize the trajectory of the tool, geometry of the parts and support system, thus boosting the use of flexible fixtures. Finally, results have been analyzed, discussed and compared to the available bibliography.

## 2. Materials and methods

### 2.1. *Tested parts and tools*

Several thin floor parts of different thicknesses and areas are tested. The dimensional ranges (part thickness and part area ranges) of the parts tested are listed in Table 1. Each part area has a corresponding fixture distribution, so there is a given distance between fixturing points for each part area. Since there are three different part thicknesses and three different part areas, there are nine kinds of parts tested. In addition, three parts are tested of each kind, so a total amount of 27 parts is milled.

The material is 2024-T3 aluminum alloy coming from a lamination process. This alloy is composed of aluminum (90.7%–94.7%), copper (3.8%–4.9%), magnesium (1.2%–1.8%), manganese (0.3%–0.9%) and other elements in proportions lower than 0.5%, such as chromium, iron, silicon, titanium and zinc. Its Brinell hardness is 120 and its density is 2.78 g/cm$^3$ [30]. T3 is the name of a three-stage heat treatment to harden and improve the mechanical properties of the alloy [31]. In addition, 2024-T3 aluminum alloy has excellent mechanical properties, machinability and surface finishing capability, so it is a material widely used in the aeronautical industry [32].

The milling is conducted with the part elevated. Each part is locally supported by four screws as fixturing points located at its corners to an intermediate rigid block that maintains the stability of the process. The part of higher area has a distance between the centers of fixturing points $d$ of 209 mm, which corresponds to a usual distance between vacuum cups in universal holding fixtures. The torque of each screw is 5 Nm.

All milling operations are performed in a 5-axis NC machining center Ibarmia ZV 25U600 Extreme, and employ a two flutes bull-nose tool Kendu 4400.60 with a 10 mm diameter, 30° helix angle, 18° rake angle, 9° clearance angle for the primary edge, 16° angle for the secondary edge and 2.5 mm edge radius. The use of bull-nose tools is usual within the

**Table 3 – Obtained cutting force coefficients.**

| $K_{tc}$ (N/mm$^2$) | $K_{rc}$ (N/mm$^2$) | $K_{ac}$ (N/mm$^2$) | $K_{te}$ (N/mm) | $K_{re}$ (N/mm) | $K_{ae}$ (N/mm) |
|---|---|---|---|---|---|
| 1849.26 | 238.51 | −170.82 | 22.614 | 19.881 | −14.946 |

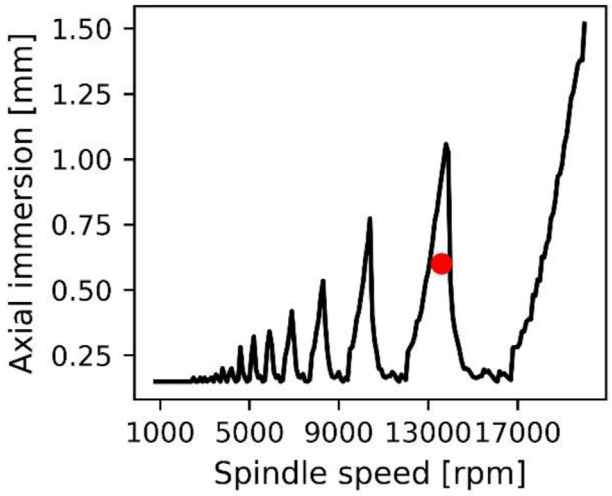


**Fig. 2 – SLD for part of geometry 85 × 85 × 2.03 mm³, and the operation point.**

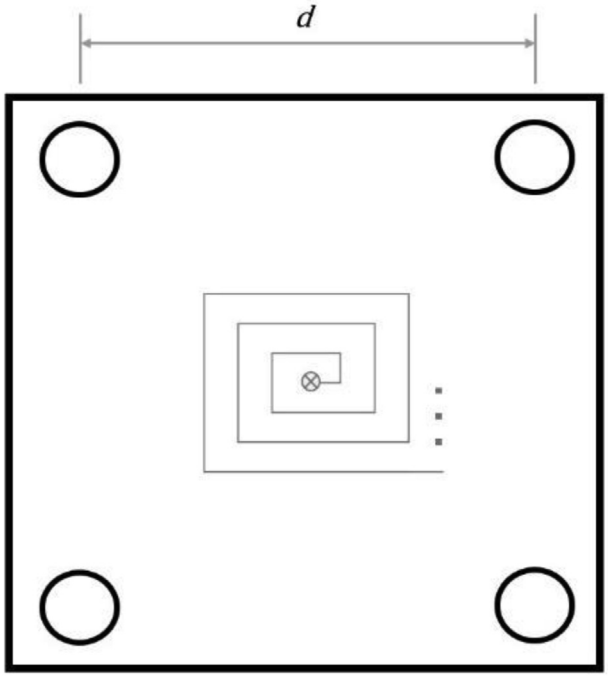


**Fig. 3 – Milling toolpath followed in the parts.**

aeronautic industry, because they can leave a fillet radius in the pockets [33]. Each part is milled with a new tool, so that any tool wear would not affect the results, as wear have considerable influence on the cutting force [34].

### 2.2. *Methodology overview*

Two consecutive stages are performed. First stage aims to determine the optimal milling conditions to be employed in the second stage, by means of the calculation of the stability lobe diagram (SLD) that shows the most stable milling conditions. Second stage employs these conditions in a full-factorial based design of experiments and pursues the determination of the cutting force predictive model for aeronautic skins, as well as the analysis of thickness error distribution. The overview of the tasks is presented in Table 2.

### 2.3. *First stage*

This stage aims to determine the optimal milling conditions, which include the milling strategy and the cutting parameters. Regarding milling strategy, the outward helicoidal toolpath is the optimum one in relation to process time, final roughness and thickness accuracy [35].

Regarding cutting parameters, SLD is provided, as it shows the combination of the spindle speed and axial immersion of the tool in the part that leads to a stable milling. SLD is calculated based on cutting coefficients and Frequency Response Function (FRF) [36].

The three-dimensional model [37,38] and a mechanistic approach [39,40] are employed to calculate the SLD.

Nevertheless, two phenomena affect SLD. On the one hand, stability lobes of parts vary during milling due to the reduction of mass and stiffness caused as a consequence of material removal, which is relatively high [41]. On the other hand, different SLDs may be needed as different part geometries are tested. However, different spindle speeds may have different thermal affections on the spindle, and therefore to the final thickness achieved [42], so in order to neutralize this effect it has been decided to maintain constant both the axial immersion of the tool and the spindle speed in all the tests, guaranteeing maximum stability at the beginning of the milling for the part of area 85 × 85 mm² and 2.03 mm thick. This kind of parts has also been tested in several studies [43,44]. Thus, a nominal axial immersion of 0.6 mm is selected, and the spindle speed would be the most stable one for that test condition according to the SLD.

In aeronautic skin milling, since the stiffness of the part throughout thickness direction is lower than the stiffness of the tool, vibration is mainly dominated by the dynamic properties and modes of the skin [45]. Consequently, SLD is calculated considering both the FRF of the tool and the FRF of the part in the thick direction [7]. As shown in Fig. 1, the accelerometer is placed below the part, at its center, since this is the point where the stiffness of the part is lower [46].

**Table 4 – Milling conditions for the parts.**

| | |
|---|---|
| Axial immersion ($a_p$) | 0.6 mm |
| Radial immersion ($a_e$) | 50% |
| Spindle speed | 13,700 rpm |
| Feed per tooth ($f_z$) | 0.1 mm |

**Table 5 – Experimental dimensional parameters.**

| Parameter | Level 1 | Level 2 | Level 3 |
|---|---|---|---|
| Part thickness ($h$) | 2.03 mm | 3.18 mm | 4.83 mm |
| Distance between fixturing points ($d$) | 69 mm | 139 mm | 209 mm |

Bull-nose end mills as the employed tool have a variable lead edge angle from 0° to 90°. This non-linearity can be simplified assuming a constant mean value for this angle [47]. In the current case a constant value of 20° is employed, as it corresponds to an axial immersion of 0.6 mm [44].

Cutting coefficients are obtained performing grooving tests at a rigid block of the same material with three different axial immersions and feed per tooth and applying the mechanistic model inversely. They are listed in Table 3.

The calculated SLD is shown in Fig. 2. Under the lobe line the milling is considered stable. Thus, the optimal spindle speed for an axial immersion of the tool of 0.6 mm is 13,700 rpm. The feed per tooth $f_z$ is set at 0.1 mm/tooth.

### 2.4. Second stage

The optimal milling conditions calculated in the first stage are listed in Table 4. They correspond to a finishing operation. In the most extreme case, the ratio of final thickness to part side is lower than 0.6%.

These conditions are employed for a dry pocket face end-milling following a square outward helicoidal toolpath in each part, as shown in Fig. 3. Toolpaths corresponding to parts of higher area comprise more straight cutting paths (33 paths in parts of $d = 69$ mm, 85 paths in parts of $d = 139$ mm and 145 paths in parts of $d = 209$ mm). The resulting tool spin frequency is 228.3 Hz and the tooth passing frequency is 456.6 Hz. Since the same milling conditions are employed for all the parts, they only differ in their geometry.

The purpose of this stage is the analysis of thickness error distribution, as well as the determination of the cutting force predictive model for aeronautic skins taking an empirical approach. So, a full-factorial methodology is carried out for the experiments, testing two parameters with three levels of each parameter (see Table 5).

### 2.5. Measurement instruments

Cutting forces are monitored with a Kistler 9257B dynamometer table. The FRF is obtained employing a PCB impact hammer model 086C03 and a cubic PCB accelerometer model 352A21, whose sensitivity is 1.041 mV/(m/s$^2$) and has 1–10,000 Hz measuring range. Thus, the hammer causes an excitation and the accelerometer measures the corresponding vibration response [48].

Cutting forces and FRF are registered and pre-processed in a OR35 analyzer/recorder instrument with NVGATE software (OROS).

The thickness distributions of the parts are measured in final parts with an Olympus Panametrics-NDT 35DL ultrasonic probe.

**Table 6 – Suitability of process force data for an ANOVA.**

| Assumption | Parameter | Values |
|---|---|---|
| Normal distribution | SW | 0.962 |
| | p-value | 0.422 |
| Homogeneity of variance | Levene | 0.762 |
| | p-value | 0.64 |

**Table 7 – ANOVA of process force.**

| Factor | Parameter | Values |
|---|---|---|
| $h$ | F-value | 0.389 |
| | p-value | 0.684 |
| $d$ | F-value | 8.806 |
| | p-value | 0.002 |
| $h \bullet d$ | F-value | 2.496 |
| | p-value | 0.082 |

Both forces and final thicknesses are measured in the middle of each straight cutting path (Fig. 4). It is considered the most stable and representative zone of the milling operation, thus avoiding the change on cutting direction that takes place at the beginning and end of each cutting path, where two teeth of the mill simultaneously engage the part.

Also, only cutting paths perpendicular to lamination direction are considered, in order to neutralize the possible effect that lamination could have on milling.

## 3. Results and discussion

### 3.1. Effect of material removal on natural frequency

Milling causes a reduction of mass and stiffness of the parts, which influences their dynamic behavior, as it leads to a corresponding change in their natural frequencies [49], which usually is a decrease [50]. Overall, it means that, regarding the evolution of natural frequency, the reduction of stiffness as consequence of the milling prevails over the reduction of mass. In Fig. 5 the evolution of the first natural frequency of each part is shown, before and after milling. Three parts have been milled of each initial thickness $h$ and distance between fixturing points $d$. It must be noted that the first natural frequency of the parts whose distance between fixturing points is $d = 209$ mm and $h = 3.18$ mm is very close to the tool spin frequency (228.3 Hz).

### 3.2. Effect of part geometry on process force

In order to analyse the effect of the initial part geometry and setup (initial thickness $h$ and distance between fixturing

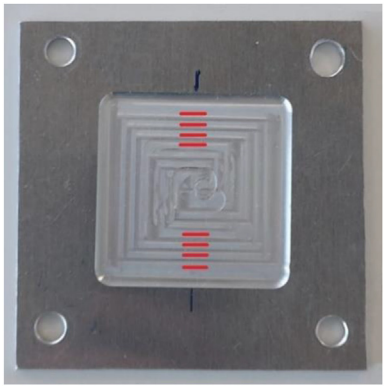

**Fig. 4 – Thickness and force measurement lines in a final part.**

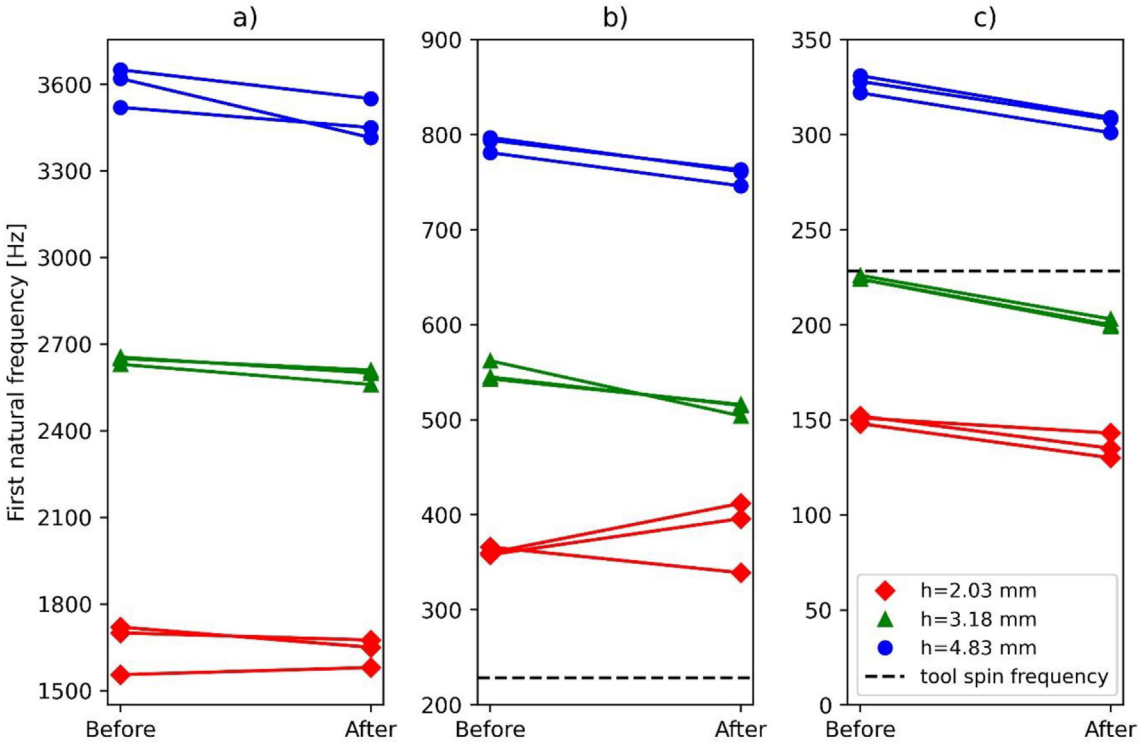


**Fig. 5 – First natural frequency of each part before and after milling. a) $d = 69$ mm. b) $d = 139$ mm. c) $d = 209$ mm.**

points $d$) on milling process force, an Analysis of Variance (ANOVA) is performed. This a well-known technique, widely employed in similar studies, although focused on cutting parameters [14] or tool geometry [51].

The assumption that data is normally distributed is checked by means of Shaphiro-Wilk test, and the assumption of variance homogeneity is checked by Levene test. A confidence interval of 95% ($\alpha = 0.05$) is set. The results of these statistical tests can be observed in Table 6. As their p-values are over $\alpha$, data is suitable for an ANOVA.

ANOVA determines the factors affecting process force. The null hypothesis is that the factors or their combination have no influence over process force. As shown in Table 7, it can be stated with a 90% of confidence that the distance between fixturing points $d$ is the main parameter affecting process force; as well as its combination to initial part thickness, which can be considered as related to the volume or the mass of the part.

As it can be observed in Fig. 6, mean and range of process forces vary according to thickness and distance between fixturing points, so both should be considered in order to achieve lower forces and a more stable milling.

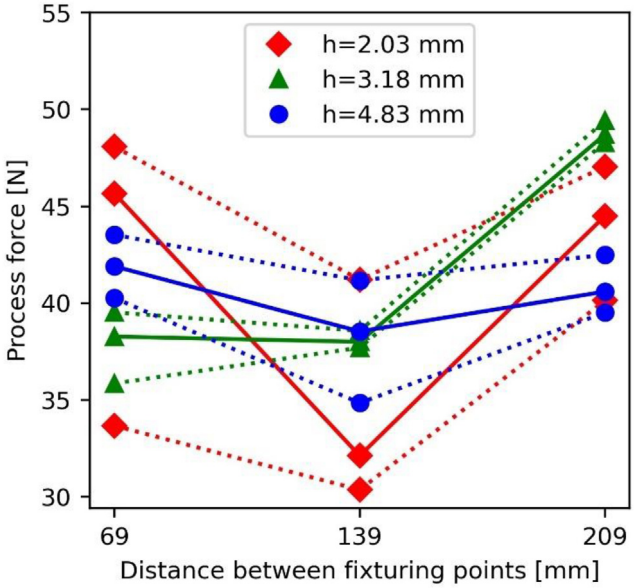


**Fig. 6 – Initial part thickness and distance between fixturing points effects on process mean force.**

### 3.3. *Effect of part geometry on final thickness mean error*

In order to analyse the effect of the initial part geometry and setup (initial thickness $h$ and distance between fixturing points $d$) on final thickness mean error, an Analysis of Variance (ANOVA) is performed. Final thickness error is defined as

**Table 8 – Suitability of real thickness data for an ANOVA.**

| Assumption | Parameter | Values |
|---|---|---|
| Normal distribution | SW | 0.953 |
| | p-value | 0.275 |
| Homogeneity of variance | Levene | 0.431 |
| | p-value | 0.886 |

**Table 9 – ANOVA of final thickness error.**

| Factor | Parameter | Values |
|---|---|---|
| $h$ | F-value | 3.634 |
| | p-value | 0.0485 |
| $d$ | F-value | 33.898 |
| | p-value | <0.001 |
| $h \bullet d$ | F-value | 4.68 |
| | p-value | 0.01 |

the deviation from the nominal final thickness pursued. Final thickness mean error is calculated as the mean value of the final thickness errors of the cutting paths.

The assumption that data is normally distributed is checked by means of Shaphiro-Wilk test, and the assumption of variance homogeneity is checked by Levene test. A confidence interval of 95% ($\alpha = 0.05$) is set. The results of these statistical tests can be observed in Table 8. As their p-values are over $\alpha$, data is suitable for an ANOVA.

Aiming to determine the factors affecting final thickness error, an ANOVA is conducted. The null hypothesis is that the factors or their combination have no influence over final thickness achieved. As shown in Table 9, it can be stated with a 90% of confidence that the null hypothesis is false and that all the factors affect the final thickness error.

As it can be observed in Fig. 7, low initials thicknesses entail higher variability in errors, and as long as distance between fixturing points increases, thickness mean error also increases, almost lineally. Such increasing of thickness mean error is related not only to the lower stiffness that higher distances between fixturing points entail, but also to the higher milling operation time, which could lead to a higher thermal expansion of the spindle. This is an influencing parameter that increases the final thickness mean error [43].

The parts whose geometry is $h = 3.18$ mm and $d = 209$ mm exhibits a remarkably higher final mean error, since their first natural frequency coincides with the tool spin frequency. However, as shown in Fig. 8, its thickness mean error corresponding only to the first 33 straight cutting paths of the toolpath is not so high. The reason could be that at the beginning of the milling first natural frequency of this part still differs to the tool spin frequency. Conversely, the rest of the parts exhibit a thickness mean error corresponding to these initial cutting paths very similar to the one corresponding to the entire toolpath. It means that tool position does not significantly affect thickness error. However, a deeper analysis regarding tool position and its effect on thickness error is carried out.

### 3.4. *Effect of tool position on thickness error*

Fig. 9, Figs. 10 and 11 show the effect that the tool position along the cutting toolpath causes on thickness error. Each column of each figure shows the three milled parts of the same initial thickness $h$ and the same distance between fixturing points $d$.

Overall, all the parts exhibit a higher error at the center, due to the initial drilling, as well as to the lower stiffness at this point [46]. Nevertheless, for each part, the thickness error is constant in the remaining paths, so it could be compensated prior to milling selecting proper milling parameters. One important exception is the part where distance is $d = 209$ mm (Fig. 11), particularly the case of thickness $h = 3.18$ mm. This is the mentioned case in which the first natural frequency of the part coincides with the tool spin frequency. It causes an extremely high and very variable thickness error, which makes compensation extremely difficult. The pattern of thickness error that this case exhibits may be related to the alternative pass of the mill tool through nodes and antinodes, which affects modal response of the part [52].

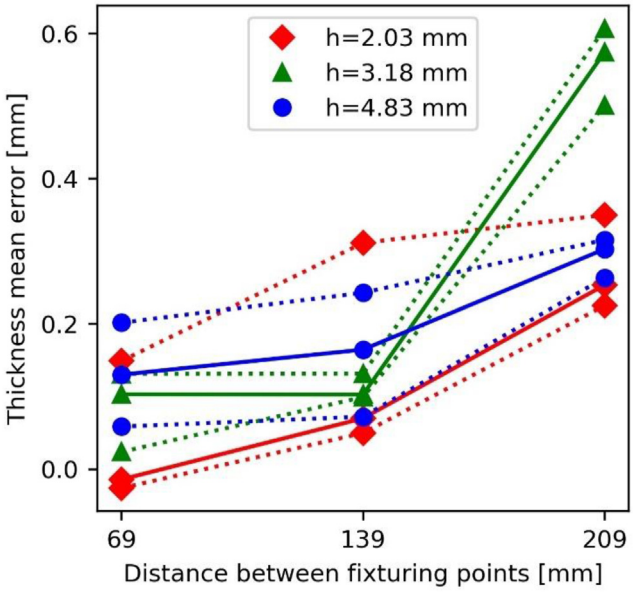


**Fig. 7 – Initial part thickness and distance between fixturing points effects on thickness mean error.**

Overall, Figs. 9, Figs. 10 and 11 probe that tool position ought to be taken into account when an excitation of modes is expected in order to reduce thickness error, but it is not a key parameter regarding thickness error in the remaining cases.

### 3.5. *Process force model*

An empirical approach is followed in order to provide a suitable force model able to relate cutting process forces to milling parameters and geometry of parts. This model has to consider milling parameters, as they strongly influence cutting force [53]. Consequently, milling parameters are grouped around the material removal rate (MRR), as shown in eq. (1), where S is spindle speed, $a_p$ is the axial immersion of the tool, $a_r$ is the radial immersion, Z is the number of teeth of the tool and $f_z$ is the feed per tooth [14].

$$MRR = Z \cdot f_z \cdot a_p \cdot a_r \cdot S \tag{1}$$

Data has been randomly split and the 85% of the data has been employed as training data for developing the model, and the 15% as testing data. The developed model is a linear regression that allows the prediction of the module of the cutting process force at each point of the toolpath, taking into account not only milling parameters but also tool position and material loss. This mathematical model of the module of the resultant cutting force is shown in eq. (2).

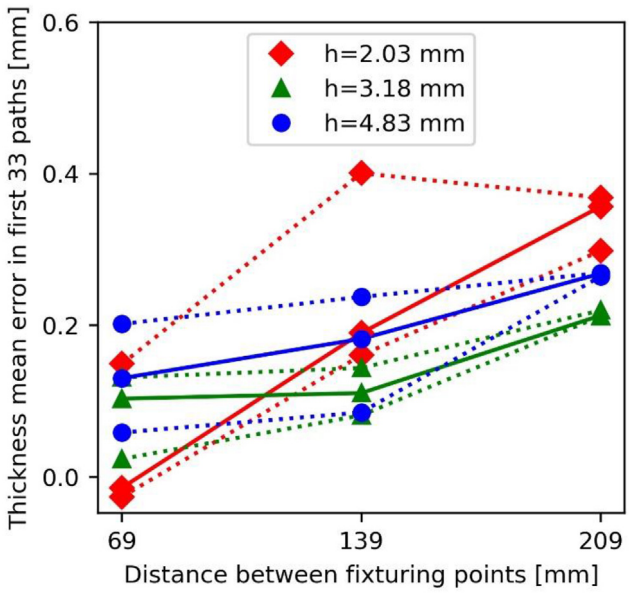


**Fig. 8 – Initial part thickness and distance between fixturing points effects on thickness mean error in first 33 paths.**

In the model, material removal rate is expressed in $mm^3/min$. $D_{near}$ is the ratio of the distance from the considered point of the toolpath to the nearest fixturing points regarding the distance from the center of the part. $V_{rem}$ is the ratio of the remaining volume of the part at the considered point of the toolpath regarding the initial part volume. The model is valid for the interval where $V_{rem} > 0.8$ and $D_{near} > 0.7$, where the tests have been performed.

$$\begin{aligned}\widehat{F} = &-562.69 - 0.00625\cdot MRR + 576.4\cdot V_{rem} + 789.4\cdot D_{near}\\ &+ 14.58\cdot h + 0.0028\cdot d^2 - 0.009\cdot MRR\cdot D_{near}\\ &+ 0.0162\cdot MRR\cdot V_{rem} - 5\cdot 10^{-5}\cdot MRR\cdot h + 1.66\cdot 10^{-9}\cdot MRR\cdot d^2\\ &- 780\cdot V_{rem}\cdot D_{near} + 5.62\cdot h\cdot D_{near} + 0.002\cdot d^2\cdot D_{near}\\ &- 19.1\cdot h\cdot V_{rem} - 0.0048\cdot d^2\cdot V_{rem} + 2.4\cdot 10^{-5}\cdot d^2\cdot h\end{aligned} \quad (2)$$

Even though other developed force models for similar kinds of parts are based on potential regressions [14,39], no significant differences regarding accuracy have been found for the present case. The accuracy of the developed model is checked by means of two statistical parameters, which are the mean absolute error (MAE) and the mean absolute percentage error (MAPE). MAE measures the average absolute deviation between forecasted and real force values, and MAPE measures the relative deviation. They are defined according to eq. (3) and eq. (4), where $N$ is the total amount of the available data [54].

$$MAE = \frac{\sum_{i=1}^{N}|F_i - \widehat{F}_i|}{N} \quad (3)$$

$$MAPE = \frac{100}{N}\cdot\sum_{i=1}^{N}\left|\frac{F_i - \widehat{F}_i}{F_i}\right| \quad (4)$$

These statistical parameters are calculated for the testing data. The results are $MAE = 2.4\ N$ and $MAPE = 5.6\%$. Thus, the model allows an accurate forecasting of forces, considering the high variability that process forces undergo as consequence of low stiffness.

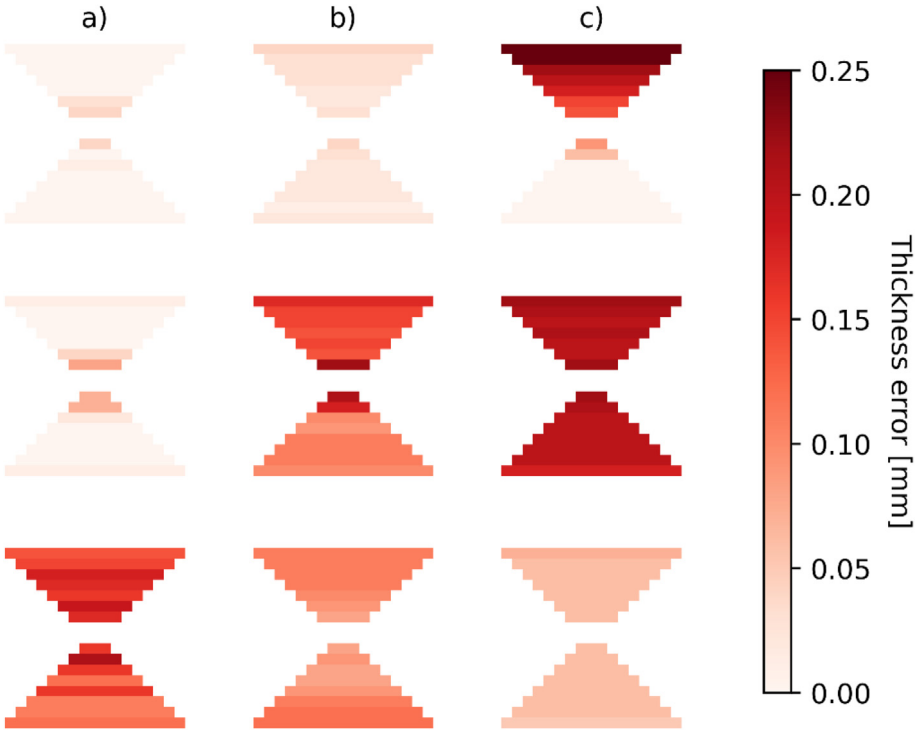


**Fig. 9 – Thickness error in each cutting path for parts whose distance between fixturing points is $d = 69$ mm. a) $h = 2.03$ mm. b) $h = 3.18$ mm. c) $h = 4.83$ mm.**

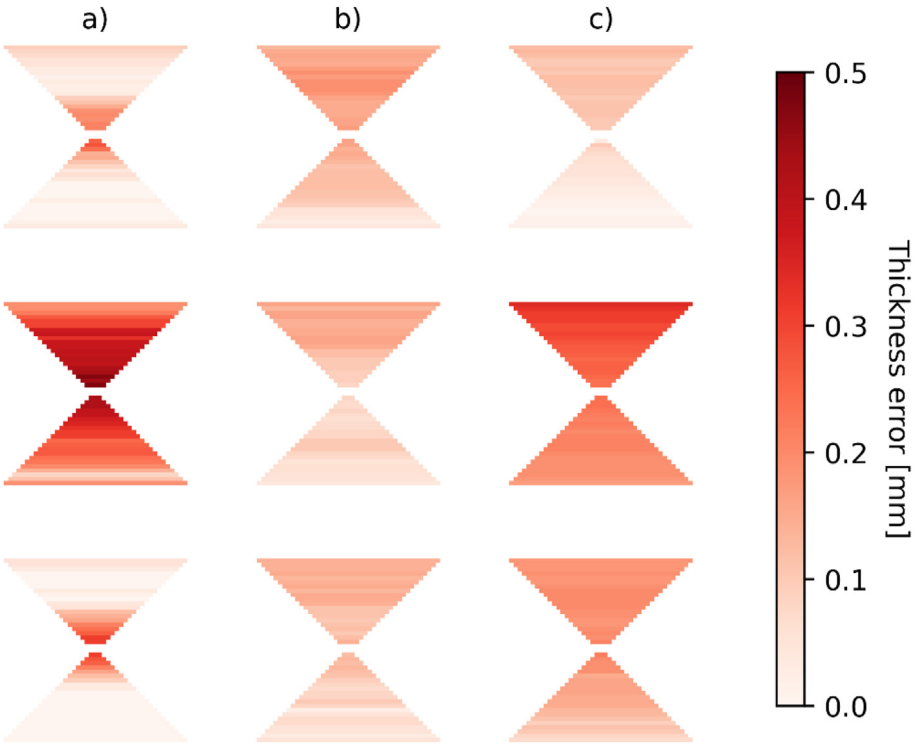


**Fig. 10 – Thickness error in each cutting path for parts whose distance between fixturing points is $d = 139$ mm. a) $h = 2.03$ mm. b) $h = 3.18$ mm. c) $h = 4.83$ mm.**

In Fig. 12, experimental (red dots) and forecasted (green triangles) values of process force module are shown. Also, these values are compared to the ones obtained according to an existing force model for a fully supported part [43], shown as a blue line.

It is known that a reduction of stiffness causes a reduction of cutting forces [55]. This fact is confirmed in the present case, where according to the models the cutting forces in a part held only at their corners are lower than the ones expected for a fully supported part, which has higher stiffness.

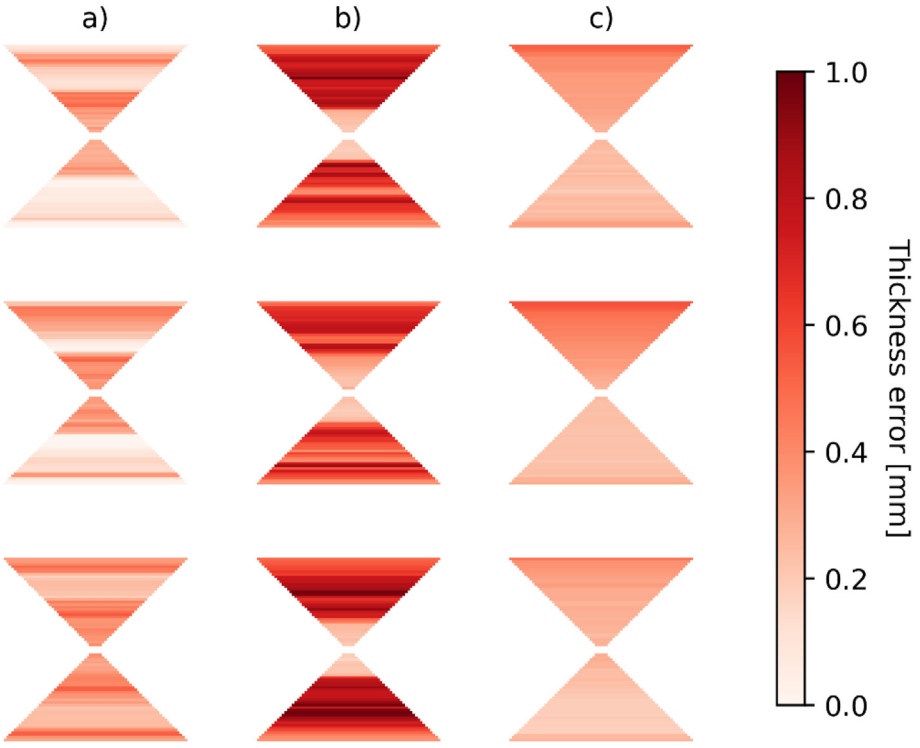


**Fig. 11 – Thickness error in each cutting path for parts whose distance between fixturing points is $d = 209$ mm. a) $h = 2.03$ mm. b) $h = 3.18$ mm. c) $h = 4.83$ mm.**

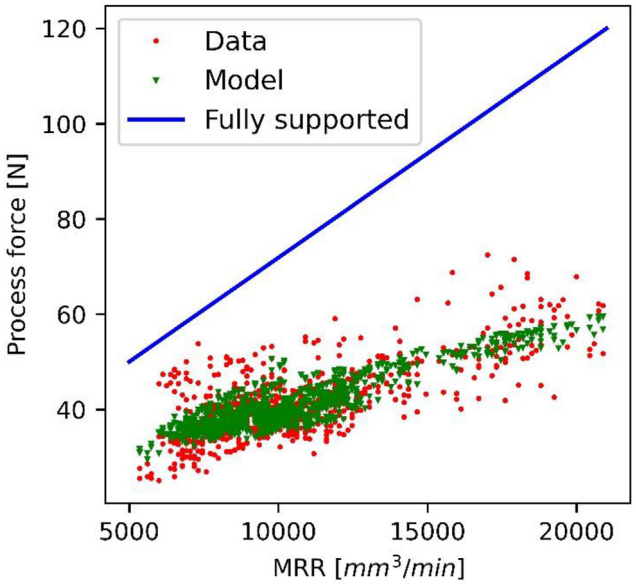


**Fig. 12 – Process force module experimental data (red dots) and predicted values according to the developed model (green triangles).**

Furthermore, in the milling of a part held only at their corners the relationship between material removal rate and process force is softer, since in the considered interval the slope of the regression for fully supported parts is close to 4.7, and the slope of the regression for simply screwed ones is close to 1.7. In addition, in the case of simply screwed parts this relation is affected not only by the material removal rate, but also by part geometry and tool position, which also causes a higher variability in process force values.

## 4. Conclusions

In this work the potential of flexible and reconfigurable holding fixtures is analyzed, where parts are milled without back support. The analysis is focused on cutting process force and final thickness achieved in the milling of ultra-low stiffness aluminum alloy parts, which is a usual situation in the aeronautic industry. The main outcomes of the paper are as follows:

(1) Tool spin frequency should be different than the first natural frequency of the part, in order to avoid excessive vibrations that cause high and irregular thickness error. Consequently, the FRF of the part should be obtained prior to milling, taking into account that it changes over time due to material loss, which causes a reduction of both mass and stiffness. It has been experimentally proven that this reduction of mass and stiffness causes a corresponding reduction of the natural frequencies of the parts.
(2) Part final thickness error is mainly affected by the distance between fixturing points, as well as by the initial part thickness. Consequently, as long as natural frequencies are not excited, thickness error is almost constant and not affected by the tool position, but only by the initial geometry and fixtures distribution of the part, so it can be reduced selecting proper milling conditions.
(3) Milling process force is mainly affected by the distance between fixturing points and the initial part thickness, as well as by the part material loss and tool position. It probes the high variability that milling forces experienced in a situation of such a low rigidity and the high number of involved factors, which makes force models developed for fully supported parts not applicable for them. Consequently, a predictive and comprehensive force model is provided considering milling parameters, initial part geometry, fixturing points distance and tool position:

$$\begin{aligned}\widehat{F} = &-562.69 - 0.00625\cdot MRR + 576.4\cdot V_{rem} + 789.4\cdot D_{near}\\ &+ 14.58\cdot h + 0.0028\cdot d^2 - 0.009\cdot MRR\cdot D_{near}\\ &+ 0.0162\cdot MRR\cdot V_{rem} - 5\cdot 10^{-5}\cdot MRR\cdot h + 1.66\cdot 10^{-9}\cdot MRR\cdot d^2\\ &- 780\cdot V_{rem}\cdot D_{near} + 5.62\cdot h\cdot D_{near} + 0.002\cdot d^2\cdot D_{near}\\ &- 19.1\cdot h\cdot V_{rem} - 0.0048\cdot d^2\cdot V_{rem} + 2.4\cdot 10^{-5}\cdot d^2\cdot h\end{aligned}$$

The model has a mean average error of 2.4 N and a mean average percentage error of 5.6%, so it can be employed for selecting suitable cutting conditions, toolpaths, fixtures position and initial part geometry, leading to lower milling process forces, thus boosting the use of universal holding fixtures.

## Declaration of Competing Interest

The authors declare that they have no known competing financial interests or personal relationships that could have appeared to influence the work reported in this paper.

## Acknowledgements

Financial support from the Basque Government under the ELKARTEK Program (EKOHEGAZ project, grant number KK-2021/00092) is gratefully acknowledged by the authors.

## REFERENCES

[1] Yücel A, Yıldırım ÇV, Sarıkaya M, Çirin Ç, Kıvak T, Gupta MK, et al. Influence of MoS2 based nanofluid-MQL on tribological and machining characteristics in turning of AA 2024 T3 aluminum alloy. J Mater Res Technol 2021;15:1688–704. https://doi.org/10.1016/j.jmrt.2021.09.007.
[2] Del Sol I, Rivero A, Norberto L, Gamez AJ. Thin-wall machining of light alloys: a review of models and industrial approaches. Materials 2019;12:2012. https://doi.org/10.3390/ma12122012.
[3] Bi Q, Huang N, Zhang S, Shuai C, Wang Y. Adaptive machining for curved contour on deformed large skin based

on on-machine measurement and isometric mapping. Int J Mach Tool Manufact 2019;136:34–44. https://doi.org/10.1016/j.ijmachtools.2018.09.001.
[4] Zhu L, Liu C. Recent progress of chatter prediction, detection and suppression in milling. Mech Syst Signal Process 2020;143:106840. https://doi.org/10.1016/j.ymssp.2020.106840.
[5] Herranz S, Campa FJ, De Lacalle LNL, Rivero A, Lamikiz A, Ukar E, et al. The milling of airframe components with low rigidity: a general approach to avoid static and dynamic problems. Proc Inst Mech Eng Part B J Eng Manuf 2005;219(11):789–801. https://doi.org/10.1243/095440505X32742.
[6] Slamani M, Chatelain JF, Il A, Balazinski M. Statistical analysis and modeling of temperature distribution during various milling operations of thin walled aircraft parts. Phys A 2021;570:125842. https://doi.org/10.1016/j.physa.2021.125842.
[7] Arnaud L, Gonzalo O, Seguy S, Jauregi H, Peigné G. Simulation of low rigidity part machining applied to thin-walled structures. Int J Adv Manuf Technol 2011;54(5–8):479–88. https://doi.org/10.1007/s00170-010-2976-9.
[8] Huang C-Y, Wang J-JJ. A pole/zero cancellation approach to reducing forced vibration in end milling. Int J Mach Tool Manufact 2010;50(7):601–10. https://doi.org/10.1016/j.ijmachtools.2010.03.011.
[9] Yuan S, Fan X. Developments and perspectives on the precision forming processes for ultra-large size integrated components. Int J Extrem Manuf 2019;1:022002. https://doi.org/10.1088/2631-7990/ab22a9.
[10] Bao Y, Dong Z, Kang R, Li Z, Yuan Y. Milling force and machining deformation in mirror milling of aircraft skin. Adv Mater Res 2016;1136:149–55. https://doi.org/10.4028/www.scientific.net/amr.1136.149.
[11] Gameros A, Lowth S, Axinte D, Nagy-Sochacki A, Craig O, Siller HR. State-of-the-art in fixture systems for the manufacture and assembly of rigid components: a review. Int J Mach Tool Manufact 2017;123:1–21. https://doi.org/10.1016/j.ijmachtools.2017.07.004.
[12] Mahmud A, Mayer JRR, Baron L. Magnetic attraction forces between permanent magnet group arrays in a mobile magnetic clamp for pocket machining. CIRP J Manuf Sci Technol 2015;11:82–8. https://doi.org/10.1016/j.cirpj.2015.08.005.
[13] Kolluru K, Axinte D. Novel ancillary device for minimising machining vibrations in thin wall assemblies. Int J Mach Tool Manufact 2014;85:79–86. https://doi.org/10.1016/j.ijmachtools.2014.05.007.
[14] Rubio-Mateos A, Rivero A, Ukar E, Lamikiz A. Influence of elastomer layers in the quality of aluminum parts on finishing operations. Metals 2020;10:289. https://doi.org/10.3390/met10020289.
[15] Meshreki M, Attia H, Kövecses J. Development of a new model for the varying dynamics of flexible pocket-structures during machining. J Manuf Sci Eng Trans ASME 2011;133(4):1–14. https://doi.org/10.1115/1.4004322.
[16] Bumgarner K, Lebakken C, Vando C, Reddie W, Jacovetti G. Patent. 0 U S Jpn Outlook 2011;8(79):578. B2.
[17] Do MD, Son Y, Choi H-J. Optimal workpiece positioning in flexible fixtures for thin-walled components. Comput Des 2018;95:14–23. https://doi.org/10.1016/J.CAD.2017.09.002.
[18] Hu F, Li D. Process planning and simulation strategies for perimeter milling of thin-walled flexible parts held by reconfigurable fixturing system. Proc - 3rd Int Conf Meas Technol Mechatronics Autom ICMTMA. 2011;2:922–6. https://doi.org/10.1109/ICMTMA.2011.513.
[19] Mtorres. Surface Milling Machine [cited 2022 July 7] Available from: https://mtorres.es/es/equipamientos/sistemas-de-fabricacion/machining/surface-milling.
[20] Modig. Vacuum clamping fixture UHF [cited 2022 July 7] Available from: https://www.directindustry.com/prod/modig-machine-tool/product-100307-1657266.html.
[21] Kostyrka. Universal holding fixture (UHF) Flexible Tooling System [cited 2022 July 7] Available from: https://eurotechcorp.com/wp-content/uploads/2019/07/KostyrkaUHF.pdf.
[22] CMS. CMSNA's Aluminum Skin Thickness Reduction System [cited 2022 July 7] Available from: https://www.scmgroup.com/en_BE/cmsmetal/news-events/news/news.n68614.html.
[23] Aerospace O. Flexible Tooling for Automation [cited 2020 July 7] Available from: http://onexia.com/aerospace/pdf//ONExia-Aerospace-UHF.pdf.
[24] Burdinberri. Milling of A320 HTP Elevator skins [cited 2020 July 7] Available from: http://www.burdinberri.com/es/recanteo-revestimientos-a320-htp-elevator.
[25] Rubio-Mateos A, Rivero A, Del Sol I, Ukar E, Lamikiz A. Capacitation of flexibles fixtures for its use in high quality machining processes: an application case of the industry 4.0 paradigm. Dyna 2018;93(1):608–12. https://doi.org/10.6036/8824.
[26] Junbai L, Kai Z. Multi-point location theory, method, and application for flexible tooling system in aircraft manufacturing. Int J Adv Manuf Technol 2011;54:729–36. https://doi.org/10.1007/s00170-010-2974-y.
[27] Hu F. Location issues of thin shell parts in the reconfigurable fixture for trimming operation. J Aero Technol Manag 2014;6(3):319–31. https://doi.org/10.5028/jatm.v6i3.321.
[28] Casuso M, Rubio-Mateos A, Antonio Veiga F, Lamikiz A. Influence of axial depth of cut and tool position in locally supported thin floor milling. Materials 2022;15:731. https://doi.org/10.3390/ma1503073.
[29] Pimenov DY, Gupta MK, Da Silva LRR, Kiran M, Khanna N, Krolczyk GM. Application of measurement systems in tool condition monitoring of Milling: a review of measurement science approach. Measurement 2022;199:111503. https://doi.org/10.1016/j.measurement.2022.111503.
[30] ASM, Aerospace Specifications Metals. Aluminum 2024-T3 [cited 2022 July 7] Available from: https://asm.matweb.com/search/SpecificMaterial.asp?bassnum=ma2024t3.
[31] García Rueda FC, Torres González J, Hernández-López JM. Differences between the untreated and treated diffusion zone in the Alclad 2024-T3 aluminum alloy and hard anodic films. Surf Coating Technol 2022;429:127939. https://doi.org/10.1016/j.surfcoat.2021.127939.
[32] André NM, Goushegir SM, Dos Santos JF, Canto LB, Amancio-Filho ST. Friction Spot Joining of aluminum alloy 2024-T3 and carbon-fiber-reinforced poly(phenylene sulfide) laminate with additional PPS film interlayer: microstructure, mechanical strength and failure mechanisms. Compos Part B 2016;94:197–208. https://doi.org/10.1016/j.compositesb.2016.03.011.
[33] Campa FJ, Lopez De Lacalle LN, Celaya A. Chatter avoidance in the milling of thin floors with bull-nose end mills: model and stability diagrams. Int J Mach Tool Manufact 2011;51(1):43–53. https://doi.org/10.1016/j.ijmachtools.2010.09.008.
[34] Guzeev VI, Pimenov DY. Cutting force in face milling with tool wear. Russ Eng Res 2011;31(10):989–93.
[35] Del Sol I, Rivero A, Salguero J, Fernández-Vidal SR, Marcos M. Tool-path effect on the geometric deviations in the machining of UNS A92024 aeronautic skins. Procedia Manuf 2017;13:639–46. https://doi.org/10.1016/j.promfg.2017.09.134.
[36] Oleaga I, Pardo C, Zulaika JJ, Bustillo A. A machine-learning based solution for chatter prediction in heavy-duty milling machines. Meas J Int Meas Confed 2018;128:34–44. https://doi.org/10.1016/j.measurement.2018.06.028.

[37] Altintas Y, Budak Erhan. Analytical Prediction of Stability Lobes in Milling 1995;44(2):357–62.
[38] Campa FJ, López de Lacalle LN, Lamikiz A, Sánchez JA. Selection of cutting conditions for a stable milling of flexible parts with bull-nose end mills. J Mater Process Technol 2007;191(1–3):279–82. https://doi.org/10.1016/j.jmatprotec.2007.03.023.
[39] Gradišek J, Kalveram M, Weinert K. Mechanistic identification of specific force coefficients for a general end mill. Int J Mach Tool Manufact 2004;44(4):401–14. https://doi.org/10.1016/j.ijmachtools.2003.10.001.
[40] Urbikain G, Alvarez A, de Lacalle LNL, Arsuaga M, Alonso MA, Veiga F. A reliable turning process by the early use of a deep simulation model at several manufacturing stages. Machines 2017;5(2). https://doi.org/10.3390/machines5020015.
[41] Yue C, Gao H, Liu X, Liang SY, Wang L. A review of chatter vibration research in milling. Chin J Aeronaut 2019;32(2):215–42. https://doi.org/10.1016/j.cja.2018.11.007.
[42] Chen JS, Hsu WY. Characterizations and models for the thermal growth of a motorized high speed spindle. Int J Mach Tool Manufact 2003;43(11):1163–70. https://doi.org/10.1016/S0890-6955(03)00103-2.
[43] Del Sol I, Rivero A, Gamez AJ. Effects of machining parameters on the quality in machining of aluminium alloys thin plates. Metals 2019;9:927. https://doi.org/10.3390/met9090927.
[44] Rubio-Mateos A, Casuso M, Rivero A, Ukar E. Vibrations characterization in milling of low stiffness parts with a rubber-based vacuum fixture. Chin J Aeronaut 2020;34(6):54–66. https://doi.org/10.1016/j.cja.2020.04.002.
[45] Wu G, Li G, Pan W, Raja I, Wang X, Ding S. A state-of-art review on chatter and geometric errors in thin-wall machining processes. J Manuf Process 2021;68:454–80. https://doi.org/10.1016/j.jmapro.2021.05.055.
[46] Campa FJ, Seguy S, Norberto L, Arnaud L, Dessein G, Aramendi G. Stable milling of thin-walled parts with variable dynamics. 6th Int Conf High Speed Mach. 2007;1. hal-03273545.
[47] Altintas Y. Analytical prediction of three-dimensional chatter stability in milling. JSME Int J Ser C Mech Syst, Mach Elem Manuf. 2001;44(3):717–23.
[48] Ma J, Zhang D, Wu B, Luo M, Chen B. Vibration suppression of thin-walled workpiece machining considering external damping properties based on magnetorheological fluids flexible fixture. Chin J Aeronaut 2016;29(4):1074–83. https://doi.org/10.1016/j.cja.2016.04.017.
[49] Shi J, Song Q, Liu Z, Ai X. A novel stability prediction approach for thin-walled component milling considering material removing process. Chin J Aeronaut 2017;30(5):1789–98. https://doi.org/10.1016/J.CJA.2017.05.011.
[50] Seguy S, Campa FJ, de Lacalla LNL, Arnaud L, Dessein G, Aramendi G. Toolpath dependent stability lobes for the milling of thin-walled parts. Int J Mach Mach Mater 2008;4(4):377–92. https://doi.org/10.1504/IJMMM.2008.023720.
[51] Bolar G, Das A, Joshi SN. Measurement and analysis of cutting force and product surface quality during end-milling of thin-wall components. Meas J Int Meas Confed 2018;121:190–204. https://doi.org/10.1016/j.measurement.2018.02.015.
[52] Thevenot V, Arnaud L, Dessein G, Cazenave-Larroche G. Influence of material removal on the dynamic behavior of thin-walled structures in peripheral milling. Mach Sci Technol 2006;10(3):275–87. https://doi.org/10.1080/10910340600902082.
[53] Pimenov DY, Guzeev VI, Mikolajczyk T, Patra K. A study of the influence of processing parameters and tool wear on elastic displacements of the technological system under face milling. Int J Adv Manuf Technol 2017;92(9–12):4473–86. https://doi.org/10.1007/s00170-017-0516-6.
[54] Rifai AP, Aoyama H, Tho NH, Md Dawal SZ, Masruroh NA. Evaluation of turned and milled surfaces roughness using convolutional neural network. Measurement 2020;161:107860. https://doi.org/10.1016/j.measurement.2020.107860.
[55] López De Lacalle LN, Lamikiz A, Sánchez JA, Fernández De Bustos I. Recording of real cutting forces along the milling of complex parts. Mechatronics 2006;16(1):21–32. https://doi.org/10.1016/j.mechatronics.2005.09.001.